PAPER

Check for updates

Bandgap lowering in mixed alloys of Cs₂Ag(Sb$_x$Bi$_{1−x}$)Br₆ double perovskite thin films†‡

Zewei Li,§*[a] Seán R. Kavanagh, [ID] §*[bcd] Mari Napari, [ID] [e] Robert G. Palgrave, [ID] [b] Mojtaba Abdi-Jalebi, [ID] [f] Zahra Andaji-Garmaroudi,[a] Daniel W. Davies, [ID] [bd] Mikko Laitinen,[g] Jaakko Julin,[g] Mark A. Isaacs, [ID] [bh] Richard H. Friend,[a] David O. Scanlon, [ID] [bdi] Aron Walsh [ID] [cj] and Robert L. Z. Hoye [ID] *[c]

Halide double perovskites have gained significant attention, owing to their composition of low-toxicity elements, stability in air and long charge-carrier lifetimes. However, most double perovskites, including Cs₂AgBiBr₆, have wide bandgaps, which limits photoconversion efficiencies. The bandgap can be reduced through alloying with Sb³⁺, but Sb-rich alloys are difficult to synthesize due to the high formation energy of Cs₂AgSbBr₆, which itself has a wide bandgap. We develop a solution-based route to synthesize phase-pure Cs₂Ag(Sb$_x$Bi$_{1−x}$)Br₆ thin films, with the mixing parameter x continuously varying over the entire composition range. We reveal that the mixed alloys (x between 0.5 and 0.9) demonstrate smaller bandgaps than the pure Sb- and Bi-based compounds. The reduction in the bandgap of Cs₂AgBiBr₆ achieved through alloying (170 meV) is larger than if the mixed alloys had obeyed Vegard's law (70 meV). Through in-depth computations, we propose that bandgap lowering arises from the type II band alignment between Cs₂AgBiBr₆ and Cs₂AgSbBr₆. The energy mismatch between the Bi and Sb s and p atomic orbitals, coupled with their non-linear mixing, results in the alloys adopting a smaller bandgap than the pure compounds. Our work demonstrates an approach to achieve bandgap reduction and highlights that bandgap bowing may be found in other double perovskite alloys by pairing together materials forming a type II band alignment.

[a]*Cavendish Laboratory, Department of Physics, University of Cambridge, JJ Thomson Avenue, Cambridge CB3 0HE, UK. E-mail: zl362@cam.ac.uk*

[b]*Department of Chemistry, University College London, 20 Gordon Street, London WC1H 0AJ, UK. E-mail: sean.kavanagh.19@ucl.ac.uk*

[c]*Department of Materials, Imperial College London, Exhibition Road, London SW7 2AZ, UK. E-mail: r.hoye@imperial.ac.uk*

[d]*Thomas Young Centre, University College London, Gower Street, London WC1E 6BT, UK*

[e]*Zepler Institute for Photonics and Nanoelectronics, University of Southampton, University Road, Southampton SO17 1BJ, UK*

[f]*Institute for Materials Discovery, University College London, Torrington Place, London WC1E 7JE, UK*

[g]*Department of Physics, University of Jyväskylä, P.O. Box 35, 40014, Finland*

[h]*HarwellXPS, Research Complex at Harwell, Harwell Science and Innovation Campus, Didcot, Oxfordshire OX11 0DE, UK*

[i]*Diamond Light Source Ltd., Diamond House, Harwell Science and Innovation Campus, Didcot, Oxfordshire OX11 0DE, UK*

[j]*Department of Materials Science and Engineering, Yonsei University, Seoul 120-749, South Korea*

† Raw data available. See DOI: 10.14469/hpc/7480

‡ Electronic supplementary information (ESI) available. See DOI: 10.1039/d0ta07145e

§ These authors contributed equally to this work.

Introduction

Despite the meteoric rise in efficiency of photovoltaics based on lead-halide perovskites,[1,2] concerns remain over the toxicity of the lead component.[3] Three of the main approaches to find lead-free alternatives are: (a) chemical substitution of Pb²⁺ with more benign metal cations;[4] (b) discovery of materials that could replicate the defect tolerance of the lead-halide perovskites;[5,6] and (c) exploration of halide materials that maintain the perovskite crystal structure. The third route has led to extensive work on double perovskites, in which the toxic Pb²⁺ cation is replaced with a pair of monovalent and trivalent cations (*e.g.*, Ag⁺ and Bi³⁺).[7–13] Double perovskites, or elpasolites, have the general formula A₂B(I)B(III)X₆, where A is a monovalent cation (such as Cs⁺ or CH₃NH₃⁺), B(I) a monovalent metal cation (such as Na⁺, Cu⁺, Ag⁺ or Au⁺), B(III) a trivalent metal cation (usually Sb³⁺, Bi³⁺ or In³⁺) and X a halide anion (Cl⁻, Br⁻ or I⁻).[7,13–15] Calculations have shown that the bandgap can be tuned over a wide range by changing the species in each atomic site. There has been particular focus on Cs₂AgBiBr₆ for photovoltaic applications, and several groups have demonstrated long charge-carrier lifetimes, which can exceed a microsecond.[13,16,17] Photovoltaic devices with Cs₂AgBiBr₆ have demonstrated high external quantum efficiencies reaching

21780 | *J. Mater. Chem. A*, 2020, 8, 21780–21788

This journal is © The Royal Society of Chemistry 2020

60%,[18] with stable performance over hundreds of hours in ambient air.[19] These promising charge transport properties, coupled with the improved stability of $Cs_2AgBiBr_6$ over lead-halide perovskites, have led to the material also being considered for photocatalytic applications.[20,21]

However, the potential of $Cs_2AgBiBr_6$ for photovoltaic and photocatalytic applications is limited by the wide bandgap (2.1–2.3 eV) and its indirect nature, which limit light absorption.[12,13,20–23] Efforts to achieve a smaller and more direct bandgap have involved alloying with Tl, but this is more toxic than Pb.[8,24] Alloying $Cs_2AgBiBr_6$ with the substantially less toxic Sb was also shown to be effective, but led to a smaller reduction in bandgap than Tl alloying.[25–27] In part, this was because the Sb-based double perovskite itself ($Cs_2AgSbBr_6$) has a wide bandgap of 1.9–2.1 eV.[11,15] Another factor was that only a maximum of 37.5% Sb could be introduced through powder melt synthesis, limiting the extent of bandgap reduction.[25] Intriguingly, mixed $Cs_2Ag(Sb_xBi_{1-x})Br_6$ alloys have exhibited a non-linear reduction in the bandgap, i.e., bandgap bowing, with increasing Sb content.[25,27] Bandgap bowing has also been found in Pb/Sn perovskite alloys, and, in this case, the bowing is pronounced, such that the mixed alloy exhibits a smaller bandgap than either of the pure Pb- or Sn-based compounds.[28–30] An important question would be whether a similar phenomenon occurs in $Cs_2Ag(Sb_xBi_{1-x})Br_6$ alloys.

So far, there is a lack of understanding of the extent of bandgap bowing in Sb–Bi double perovskite alloys and whether the mixed compositions could exhibit a smaller bandgap than the pure compounds. This requires the full composition range in $Cs_2Ag(Sb_xBi_{1-x})Br_6$ alloys to be synthesized. However, synthesizing phase-pure $Cs_2AgSbBr_6$ is challenging, particularly in thin film form. This is due to the high formation energy of $Cs_2AgSbBr_6$ and the small ionic radius of Sb^{3+} relative to Bi^{3+}.[31] Recently, Liu et al. synthesized thin films of $Cs_2Ag(Sb_xBi_{1-x})Br_6$ alloys by dipping their substrates in a heated solution of the precursor salts dissolved in dimethyl sulfoxide (DMSO).[27] But they were only able to achieve up to 75% Sb alloying and were not able to synthesize the pure Sb-based compound. Colloidal nanocrystal synthesis routes have been found to be more successful in growing less thermodynamically-favored compounds (e.g., iodide-based double perovskites, which have a positive heat of formation). Yang et al. recently developed a route to grow $Cs_2AgSbBr_6$ nanocrystals.[31] But it is also desirable to achieve phase-pure $Cs_2AgSbBr_6$ as bulk thin films, which do not have carriers confined within individual grains, as is the case for nanocrystals bound with long-chain ligands.

In this work, we achieved the synthesis of Sb–Bi double perovskite alloys over the entire composition range in thin film form. We found that the mixed alloys have a lower bandgap than the pure Bi- and Sb-based double perovskites, with similar pronounced nonlinear bandgap behavior to that found in lead–tin perovskite alloys.[28–30] Through X-ray diffraction (XRD) and Rutherford Backscattering Spectrometry (RBS), we found all films to be phase-pure, with the thin film composition in the bulk matching the ratio of elements in the precursor solution. We used Photothermal Deflection Spectroscopy (PDS) to accurately determine how the indirect bandgap and electronic disorder in Sb–Bi double perovskite alloys changed with composition. The electronic structure and band positions were calculated by Density Functional Theory (DFT) to provide insight into the origins of the bandgap lowering observed in the Sb–Bi double perovskite alloys.

Results and discussion

Synthesis and verification of composition

$Cs_2Ag(Sb_xBi_{1-x})Br_6$ thin films were synthesized by solution processing. The CsBr, AgBr, $SbBr_3$ and $BiBr_3$ precursors were mixed according to their stoichiometric ratio in DMSO with a concentration of 0.5 mol L^{-1}. In contrast to the dipping method used by Liu et al.,[27] we used a lower annealing temperature and shorter annealing time (detailed in the Experimental section in the ESI‡), which may have contributed to the successful synthesis of phase-pure $Cs_2AgSbBr_6$. Photographs of the films (approx. 200 nm thickness in all cases) are shown in Fig. 1a, and it was observed that the mixed compositions have a deeper color. To determine the bulk composition of the films, we performed RBS measurements (Fig. 1b and Table 1). It was found that the Sb/Bi ratio from the RBS measurements matched the stoichiometry in the precursor solution, deviating from the nominal precursor stoichiometry by up to 2.1 percentage points (Table 1). Since the Sb RBS peak is buried between two other peaks (Ag and Cs, see Fig. S1, ESI‡), the fitting and statistical uncertainties are high when the Sb concentration is low. These deviations could arise from uncertainties in the RBS measurement, as well as errors in preparing the precursor solution. These measurements therefore indicate that there is no change in the bulk composition of the thin films during crystallization. However, the presence of phase-impurities in the films below the percent-level could not be excluded.

Crystal structure and phase purity

The phase-purity of the films was determined through XRD measurements (Fig. 2a). $Cs_2AgSbBr_6$ and $Cs_2AgBiBr_6$ have the same cubic structure and space group ($Fm\bar{3}m$). The lattice constants were found to be 11.184 Å for $Cs_2AgSbBr_6$ and 11.255 Å for $Cs_2AgBiBr_6$, with a continuous variation between these

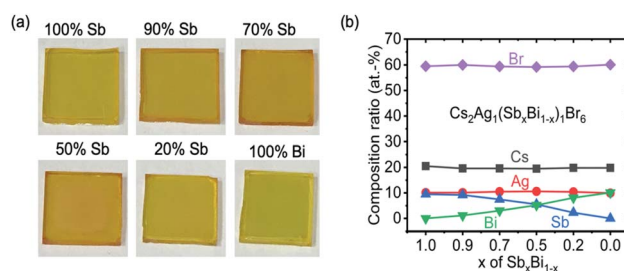**Fig. 1** (a) Photographs of the $Cs_2Ag(Sb_xBi_{1-x})Br_6$ films on glass under ambient lighting, with a thickness of approximately 200 nm. The Sb percentage labelled is that in the precursor solution. (b) Measurement of the bulk composition of $Cs_2Ag(Sb_xBi_{1-x})Br_6$ films with Rutherford Backscattering Spectrometry (fitting in Fig. S1, ESI‡).

This journal is © The Royal Society of Chemistry 2020

J. Mater. Chem. A, 2020, **8**, 21780–21788 | **21781**

Table 1 Quantification of the bulk composition of $Cs_2Ag(Sb_xBi_{1-x})Br_6$ thin films by RBS

Nominal Sb/(Sb + Bi) in precursor solution	RBS					Sb/(Sb + Bi) in film
	Cs/at%	Ag/at%	Sb/at%	Bi/at%	Br/at%	
100%	20.5	10.1	9.5	0	59.5	100%
90%	19.6	10.1	9.2	1.2	60.0	88.5%
70%	19.6	10.5	7.5	3.2	59.4	70.1%
50%	19.5	10.6	5.5	5.2	59.2	51.4%
20%	19.8	10.4	2.3	8.1	59.4	22.1%
0%	19.8	10.0	0	10.1	60.1	0%

extremes through the alloying range, as could be seen from the continuous shift in peak positions (Fig. 2b and 3d). Common phase impurities for the Sb–Bi double perovskites are $Cs_3Bi_2Br_9$ and $Cs_3Sb_2Br_9$. Both impurities have almost the same diffraction patterns with their double perovskite counterparts, but one of the main differences is a peak from $Cs_3Bi_2Br_9$ at 8.95°, or from $Cs_3Sb_2Br_9$ at 9.10°.[32] Neither impurity peaks were found to be present here. However, these XRD measurements were taken using a 1D linescan, and it is possible that the impurity peaks were not detected due to preferred orientation. We therefore performed 2D XRD measurements (Fig. S2, ESI‡). We synthesized the whole alloying range of double perovskite thin films and intentionally induced a $Cs_3(Bi,Sb)_2Br_9$ phase impurity to the films with 50% Sb. From the 2D XRD patterns, we found that the diffraction peak should be detectable by the 1D linescan if it is present. Therefore, the absence of any phase-impurities in the 1D XRD patterns in Fig. 2a shows the films to be phase-pure.

The diffraction patterns also showed no peak splitting, but the full width at half maximum (FWHM) of the pure Sb-based double perovskite and mixed alloys were larger than the Bi-based double perovskite (Fig. 2b and c). This could either be due to smaller grains or small amounts of phase segregation that could not be resolved. Scanning Electron Microscopy (SEM) measurements of the films showed that the Sb-based double perovskites and mixed alloys have smaller and less well-defined grains than the pure Bi-based double perovskite (Fig. S3, ESI‡), which is consistent with the larger FWHM in the diffraction patterns of Sb containing films. These XRD and SEM measurements, together with the RBS measurements matching the stoichiometry of the precursor solutions, are consistent with the alloys being homogeneous.

We note that previous works have reported that mixed Sb–Bi double perovskite alloys with high Sb contents have marginally lower stability. For example, Liu et al. found that $Cs_2Ag(Sb_x-Bi_{1-x})Br_6$ thin films with $x = 0.75$ had AgBr and $CsAgBr_2$

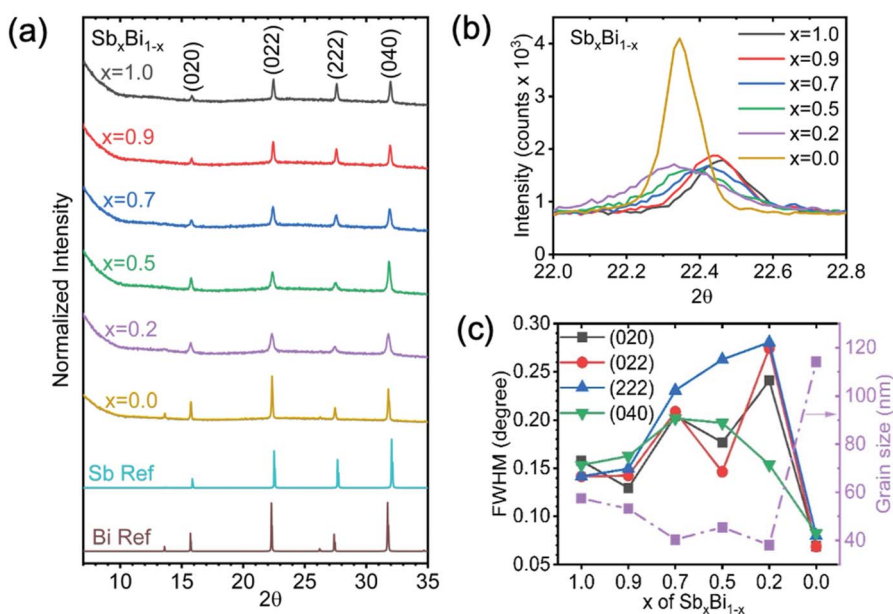**Fig. 2** (a) XRD pattern of the $Cs_2Ag(Sb_xBi_{1-x})Br_6$ films over the composition series. The reference patterns of $Cs_2AgSbBr_6$ and $Cs_2AgBiBr_6$ calculated from their crystallographic information files are denoted as Sb Ref and Bi Ref respectively.[12,15] (b) Full width half maximum (FWHM) of the (022) peak for different compositions. (c) FWHM of different diffraction peaks and the average grain size calculated using the Scherrer equation for different compositions.
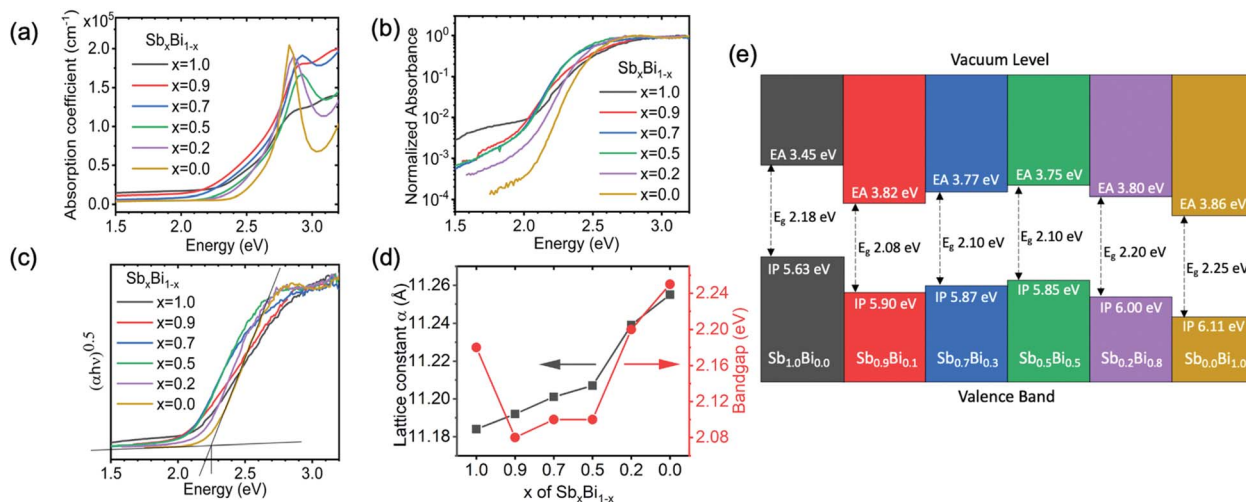
21782 | *J. Mater. Chem. A*, 2020, **8**, 21780–21788

This journal is © The Royal Society of Chemistry 2020

Fig. 3 Measurements of the bandgap of $Cs_2Ag(Sb_xBi_{1-x})Br_6$ films. (a) Absorption coefficient determined from transmittance and reflectance measurements of films deposited on glass substrates. (b) Normalized absorbance measured by PDS for films deposited on quartz substrates. (c) Tauc plot from PDS measurements. (d) Bandgap and lattice parameter of double perovskite films plotted against the Sb content in the precursor solution. The lattice parameter was acquired by fitting the XRD measurements (Fig. 2a). The bandgap was obtained from the Tauc plot constructed from the PDS data in part c. (e) Band positions of $Cs_2Ag(Sb_xBi_{1-x})Br_6$ compounds measured by ultraviolet and X-ray photoemission spectroscopy. Details of how measurements were taken and processed, the spectra fitted, and the fitted values are shown in the ESI.‡

decomposition products after 4 h annealing at 250 °C.[27] However, the diffraction peaks of these phases were small compared to the main double perovskite peaks, showing the degree of degradation to be small.[27] Sb–Bi double perovskites with lower Sb contents have been found to have comparable thermal and environmental stability as $Cs_2AgBiBr_6$.[25,27] Furthermore, the reported stability of mixed Sb–Bi double perovskites is significantly improved over $MAPbI_3$ thin films, which degrades in ambient air within 5 days[33] and decomposes to form a significant fraction of PbI_2 after 35 min at 150 °C.[34]

Absorption, bandgap and band positions

Standard optical transmittance and reflectance measurements (using a UV-visible spectrophotometer with an integrating sphere) were used to determine the absorption coefficient of the double perovskite thin films (Fig. 3a). All films showed a slow increase in the absorption coefficient for photon energies > 2 eV, before rising sharply to >10^5 cm^{-1} at >2.6 eV. An absorption coefficient exceeding 10^5 cm^{-1} at >2.6 eV is characteristic of a direct band-to-band transition. Both $Cs_2AgBiBr_6$ and Cs_2-$AgSbBr_6$ have indirect bandgaps due to the effects of the Ag d orbitals at the band-edges, and the alloys are also expected to have indirect bandgaps.[8] Therefore, to determine the indirect bandgap, we investigated the absorption onset in the lower photon energy range (i.e., between 2–2.6 eV), leaving the discussion of the absorption in the higher photon energy range to later in the paper. We observed that the alloys with 70–90% Sb showed a lower-energy absorption onset than the pure Sb- and Bi-based films. However, the indirect bandgaps resulted in the absorption coefficients being small close to the band-edge, making it difficult to accurately determine the bandgap from standard transmittance and reflectance measurements. Therefore, we performed PDS measurements, which are sensitive to

the absorbance 3–4 orders below the band-edge (operating details in the Experimental section, ESI‡).

A consequence of the high sensitivity to low absorbance is that the measurements in PDS saturate for high absorbance at >2.6 eV (Fig. 3b), and the peaks in the absorption coefficient seen in Fig. 3a are not observed in the PDS measurements plotted on a semi-logarithmic scale (see later in the paper for a discussion of these peaks). The normalized absorbance from PDS measurements at the band edge (in the range of 2–2.3 eV) is approximately 3 orders of magnitude lower than the absorbance at 2.6 eV, where the absorption coefficient is >10^5 cm^{-1} (Fig. 3a). Thus, the absorption coefficient at the band edge should be on the order of 10^2 cm^{-1}. We note that silicon, which is a typical indirect bandgap material, has an absorption coefficient of 10^2 cm^{-1} at the band edge.[35,36]

The absorption plots shown in Fig. 3b do qualitatively indicate an exponentially increasing absorption coefficient versus energy, which appears linear on a semi-logarithmic plot. The double perovskites with x ranging from 0 to 0.7 have similar slopes in their absorption onsets when plotted on a semi-logarithmic scale. For x = 0.9 and the pure Sb-based compound, the slopes are shallower. Increasing the fraction of Sb (x) from 0 (pure Bi) to 0.5 reveals a red-shift in the absorption onset. The double perovskites with x = 0.7 and x = 0.9 all have similar absorption onsets to the material with x = 0.5. These mixed alloys with x = 0.5–0.9 all have absorption onsets that are red-shifted to the pure Sb-based compound, as well as the pure Bi-based compound. Therefore, alloys with 50–90% Sb demonstrate smaller bandgaps than either of the pure end double perovskites. To extract numerical values of the bandgap and quantify their variation with composition, we fitted the PDS absorbance data using a Tauc plot, which is a plot of $(\alpha h\nu)^{1/n}$ against $h\nu$. The rationale can be seen from eqn (1)

This journal is © The Royal Society of Chemistry 2020

J. Mater. Chem. A, 2020, **8**, 21780–21788 | **21783**

$$(\alpha h\nu)^{1/n} = A(h\nu - E_g) \qquad (1)$$

where α is the absorption coefficient, h is Planck's constant, ν is the photon frequency, A is a proportionality constant, E_g is the bandgap, and $n = 2$ for an indirect bandgap.[35,36] Therefore, by plotting $(\alpha h\nu)^{0.5}$ against $(h\nu)$, the bandgap can be extracted from the intercept between the tangents fit to the absorption onset and background (Fig. 3c). From these Tauc plots, we found the system to exhibit significant bandgap bowing (Fig. 3d). The compound with $x = 0.9$ demonstrated the lowest bandgap of 2.08 eV, which is smaller than the bandgap of $Cs_2AgSbBr_6$ (2.18 eV) and $Cs_2AgBiBr_6$ (2.25 eV). We note that the bandgaps extracted from a Tauc plot can be affected by the absorptance at the band-edge and the steepness of the absorption onset. $Cs_2AgBiBr_6$ (and $Cs_2AgSbBr_6$) thin films have very low absorptance at the band-edge due to the indirect bandgap and the low quantity of material. Therefore, their bandgaps extracted from Tauc plots have tended to be higher than the bandgaps extracted in single crystals or powders, which have a significantly larger quantity of material to absorb at the band-edge.[13,16,17,25,27] In addition, it is possible that the lower bandgap extracted for the mixed alloy thin film with $x = 0.9$ than for materials with $x = 0.5$ and $x = 0.7$ (both 2.10 eV) were due to errors in the fitting process, which may have arisen in part from the lower slope in the absorption onset of the material with $x = 0.9$. Nevertheless, we emphasize that from the Tauc plots, the compounds with $x = 0.5$–0.9 all have smaller bandgaps than the pure Bi- and Sb-based compounds, and that this comparison is valid because all materials are thin films with similar thickness. The trend in bandgaps is consistent with our analysis of the PDS absorbance measurements in Fig. 3b. This is also consistent with the bandgap trend we extracted from the Tauc plots (Fig. S4, ESI‡) based on the absorption coefficient measurements (Fig. 3a). In addition, the bandgap lowering was smooth, with no switch in the bandgap from indirect to direct. This bandgap lowering behavior is similar to the Pb–Sn perovskite system and has not been previously observed in Sb–Bi double perovskites. The maximum reduction in bandgap (170 meV) compared to $Cs_2AgBiBr_6$ is larger than if the alloy system had obeyed Vegard's law and was constrained by the bandgap of $Cs_2AgSbBr_6$ (70 meV).

In addition, we measured the band positions of $Cs_2Ag(Sb_xBi_{1-x})Br_6$ over the full composition range through photoemission spectroscopy (PES; Fig. 3e). Details of how the ionization potential and electron affinity were obtained are given in the Experimental section of the ESI.‡ The fitted spectra are given in Fig. S5–S11, ESI.‡ These measurements showed that when alloying Bi into $Cs_2AgSbBr_6$, the electron affinity increased from 3.45 eV to ~3.8 eV and remained at approximately this value for the mixed alloys, which is similar to the electron affinity of $Cs_2AgBiBr_6$ (3.86 eV). The ionization potential also increased when adding Bi to $Cs_2AgSbBr_6$, but to a lesser extent than the change in the electron affinity, hence the reduction in the bandgap. The ionization potential remained at approximately 5.9 eV for $x = 0.9$ down to $x = 0.5$, before increasing to 6.11 eV for $x = 0$ (Fig. 3e). Overall, the band positions of the $Cs_2Ag(Sb_xBi_{1-x})Br_6$ alloys are compatible with the common charge transport layers for photovoltaic devices.[37] But like most other Bi-based compounds,[38] $Cs_2Ag(Sb_xBi_{1-x})Br_6$ has high ionization potentials. Achieving high open-circuit voltages will therefore require the development of hole transport layers with high work functions.

Electronic structure and bandgap lowering mechanism

To understand the atomistic origin of the bandgap lowering in the Sb–Bi double perovskites, calculations of the electronic structure were performed. The band structure and density of states for pure Sb and Bi double perovskites are shown in Fig. 4a–d. In agreement with previous literature, as well as our optical measurements in Fig. 3, both $Cs_2AgSbBr_6$ and $Cs_2AgBiBr_6$ were found to have an indirect bandgap,[8,15,25] with the valence band maximum (VBM) located at the X point and the conduction band minimum (CBM) at the L point in reciprocal space. Using relativistic hybrid density functional theory (HSE06 including spin–orbit coupling), the indirect bandgap and first direct transition of $Cs_2AgSbBr_6$ were calculated to be 1.37 and 2.60 eV, respectively. Analysis of the electron band orbital character revealed the conduction band states to be dominated by anti-bonding Sb 5p–Br 4p interactions, while the valence band states primarily arise from Sb 5s, Ag 4d and Br 4p orbital interactions. The Cs^+ cations act as spectator ions, as noted in the literature,[39] with a relatively large nearest-neighbor-ion distance to Br^-.

Likewise, the indirect bandgap and direct transition of $Cs_2AgBiBr_6$ were calculated to be 1.77 and 2.49 eV, respectively. Due to the stronger spin–orbit coupling of the Bi 6p orbitals, the direct bandgap of $Cs_2AgBiBr_6$ is slightly reduced from that of $Cs_2AgSbBr_6$, despite a larger fundamental gap, and is located at a different point in reciprocal space (X = (0.5, 0, 0.5), $cf.$ $b = (0.5, 0.38, 0.62)$ for $Cs_2AgSbBr_6$). Similarly, the conduction band states are dominated by anti-bonding interactions between the trivalent pnictogen cation (Bi 6p) and the halide anion (Br 4p) orbitals, while the valence band states primarily arise from Bi 6s, Ag 4d and Br 4p orbital interactions. Notably, the larger band gap of $Cs_2AgBiBr_6$ relative to $Cs_2AgSbBr_6$ is an interesting exception to the typical trend of decreasing bandgap upon atomic substitution with heavier members from the same periodic group, which has been observed for other perovskite materials.[11,40,41]

To delve closer to the origin of bandgap lowering, the 'natural' band offset of the two double perovskite materials was calculated following the alignment procedure of Butler et al.,[42] with the resulting electron band alignment diagram shown in Fig. 4e. Our investigations indicate a type II 'staggered gap' alignment, with a valence band offset (VBO) of 0.75 eV and a conduction band offset (CBO) of 0.34 eV ($Cs_2AgSbBr_6$ above $Cs_2AgBiBr_6$ in both cases). Typically, the energies of valence electrons become less negative as one moves down a group in the periodic table, corresponding to a decrease in ionization energies. However, for Bi^{3+} and Sb^{3+}, this is not the case, with the Bi^{3+} $6s^2$ lone pair being lower in energy than the Sb^{3+} $5s^2$ lone pair.[43] This is a result of the relativistic contraction of the Bi 6s orbital, due to its large atomic number, resulting in a more localized, lower-energy valence s orbital, compared to Sb 5s.[44]

Consequently, the more-diffuse, higher-energy Sb $5s^2$ lone-pair has a stronger interaction with the Ag 4d and Br 4p
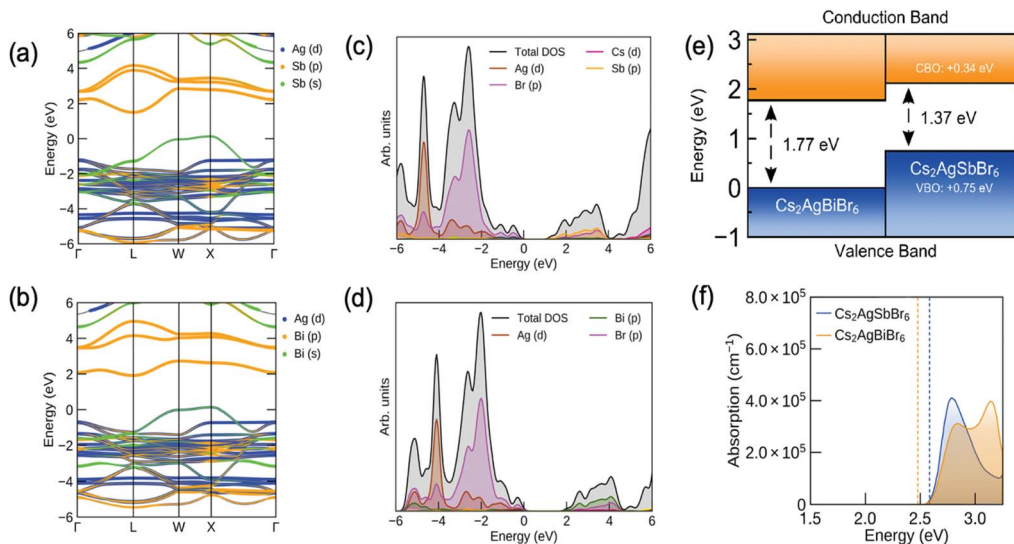
21784 | J. Mater. Chem. A, 2020, 8, 21780–21788

This journal is © The Royal Society of Chemistry 2020

Fig. 4 (a) Orbital-projected band structure of $Cs_2AgSbBr_6$. (b) Orbital-projected band structure of $Cs_2AgBiBr_6$. (c) Electronic density of states of $Cs_2AgSbBr_6$. (d) Electronic density of states of $Cs_2AgBiBr_6$. (e) Electron band alignment of $Cs_2AgSbBr_6$ and $Cs_2AgBiBr_6$. CBO = Conduction Band Offset, VBO = Valence Band Offset. (f) Calculated optical absorption plots of $Cs_2AgSbBr_6$ (blue) and $Cs_2AgBiBr_6$ (orange). Dashed vertical lines indicate the positions of optical absorption onset, corresponding to the direct band transitions of 2.60 eV for $Cs_2AgSbBr_6$ and 2.49 eV for $Cs_2AgBiBr_6$. Note that only vertical transitions are accounted for in this calculation, and the absorption from indirect transitions are not shown.

orbitals, due to a reduced energy separation of the bonding orbitals (Fig. S12, ESI‡). This produces both greater dispersion in the valence band and a higher VBM, as shown in Fig. 4e. In a similar manner, the elevated position of the CBM in Cs_2-$AgSbBr_6$ can be understood by considering the ionization energies and ionic orbital energies. While the first ionization energy of Sb is indeed larger than that of Bi, the third ionization energy (corresponding to the removal of a p electron from Sb^{2+}/ Bi^{2+}) is in fact 0.3 eV lower for Sb than for Bi,[43] indicating higher energy cationic p states. When the pnictogen elements are in the +3 oxidation state, as is the case in these materials, the third ionization energy provides an improved estimate for the energy of the unoccupied p orbitals. Hence, we argue that, in the +3 formal charge state, the Sb valence p orbitals are in fact higher in energy than those of Bi, suggesting a higher energy CBM for $Cs_2AgSbBr_6$, as witnessed in our investigations.

The origins of bandgap bowing in semiconductor alloys are typically due to chemical effects (e.g., differences in electronegativity), local size-mismatch effects or changes in the lattice parameter.[45–47] For the Pb–Sn perovskite alloy system, Im et al. attributed bandgap bowing to the combined effect of spin–orbit coupling and composition-induced phase change.[30] Snaith and coworkers proposed that the short range ordering of preferred atomic scale clusters allow the bandgap of the mixed alloy to be below that of both pure compounds.[29] In contrast, Stevanović and coworkers found that the strong nonlinearity in bandgap was primarily due to the mismatch in energy between s and p atomic orbitals of Pb and Sn.[28] The Pb–Sn alloys have a higher VBM dominated by Sn-5s and I-5p orbitals and lower CBM dominated by Pb-6p and I-5p orbitals. They found that spin–orbit coupling, structure changes and short-range ordering did not have a significant effect on bandgap bowing, and proposed

that a homogeneous structure would have improved stability over a structure with short range ordering.

In the case of $Cs_2Ag(Sb_xBi_{1-x})Br_6$, we propose that the type II staggered gap alignment between the pure compounds allows for the non-linear mixing of electronic states such that bandgaps lower than that of either pure material are obtained (Fig. 4e). Upon addition of Bi to the pure Sb double perovskite, the conduction band will be lowered because the CBM wavefunction amplitude is preferentially allocated to the Bi sites, producing a 'Bi-like', lower-energy conduction band state. The presence of Bi will also enhance spin–orbit coupling, further reducing the energy of the CBM. On the other hand, the highest energy valence band state will remain 'Sb-like', with greater wavefunction amplitude at the Sb sites yielding a VBM only slightly below that of the pure Sb material. This mixing of electronic states in the alloys to produce a low-energy CBM, dominated by Bi–Br interactions, and a high-energy VBM, dominated by Sb–Ag–Br interactions, produces bandgaps in the double perovskite alloys which are lower than that of either pure material. Indeed, this prediction is supported by electronic structure calculations for the alloys (assuming a uniform atomic distribution), which show reduced bandgaps due to the expected orbital mixing at the band edges (Fig. S13–S15 and Table S3, ESI‡). These predictions are further supported by the experimentally-determined band positions of the $Cs_2Ag(Sb_x$-$Bi_{1-x})Br_6$ compounds (Fig. 3e), which show the electron affinities of the mixed alloys to be close to $Cs_2AgBiBr_6$. The ionization potentials of the mixed alloys with $x = 0.5$–0.9 are in between those of the pure compounds. This accounts for the reduction in their bandgap compared to $Cs_2AgBiBr_6$. The reduction in the bandgaps of the $x = 0.5$–0.9 mixed alloys compared to Cs_2-$AgSbBr_6$ are due to the increase in ionization potential being

This journal is © The Royal Society of Chemistry 2020

J. Mater. Chem. A, 2020, **8**, 21780–21788 | **21785**

smaller than the increase in electron affinity when Bi is added to $Cs_2AgSbBr_6$, as discussed earlier.

Notably, this combination of a low-energy CBM with a high-energy VBM is expected to allow for enhanced doping and hence increased carrier concentrations in the alloy, relative to the pure materials.[48–50] In particular, the raised VBM, relative to pure $Cs_2AgBiBr_6$ (which has been reported as intrinsically p-type),[10,16,51] should allow for greater hole carrier concentrations in the reduced-bandgap alloy. This is supported by our X-ray photoemission spectroscopy measurements, which show a reduction in the valence band to Fermi level offset when Sb is alloyed into $Cs_2AgBiBr_6$, showing the materials to become more p-type (Table S1, ESI‡).

As the alloy mixing parameter x approaches extreme values ($x \rightarrow 0$ or $x \rightarrow 1$), the ability of the band extrema states to simultaneously adopt Bi and Sb character is diminished, hence the bandgap increases toward the pure double perovskite values. Therefore, we propose that this orbital-mixing behavior, facilitated by the type II bandgap alignment, is the origin of the non-linear, non-monotonic variation in bandgap with composition in the Sb–Bi double perovskite system.

Another possible contribution to bandgap bowing is volume deformation, whereby variation in the lattice constant upon alloying results in non-linear transformation of the electronic structure.[28] This mechanism, however, more commonly dominates in alloys involving more chemically-distinct materials than is the case here. Moreover, due to the small positive bandgap deformation potentials calculated for the Sb and Bi compounds ($\Delta E_g \sim 0.02$ eV), we rule out this mechanism. Relative to the experimentally-observed bowing (~ 0.1 eV, Fig. 3d), volume distortion alone is not the origin of bandgap bowing in this alloy system.

Finally, we return to discuss the sharp peak in the absorption coefficient of the films at >2.6 eV (Fig. 3a). This is especially evident for $Cs_2AgBiBr_6$. Previous work attributed the sharp absorption peak in $Cs_2AgBiBr_6$ to an exciton associated with the direct transition.[26,52–55] However, there is also the possibility that these features in the pure compounds and mixed alloys are due to a narrow density of states at the band-edges. To explore this possibility, we computed the absorption spectra for $Cs_2AgSbBr_6$ and $Cs_2AgBiBr_6$ without excitonic effects (Fig. 4f). These spectra were broadened by convoluting with a Gaussian peak with a FWHM of 0.15 eV. For both materials, the calculated absorption spectra exhibit peaks at 2.8 eV, in agreement with the experimental measurements. These peaks arise from the relatively-weak dispersion of the electron bands at the CBM and VBM of the materials (Fig. 4a and b), yielding peaks in both the density of states (Fig. 4c and d) and thus the optical absorption (Fig. 4f). This strongly suggests that the peaks observed in the experimental UV-visible measurements are the result of direct transitions between the relatively-flat electron bands. That said, the exciton binding energy of $Cs_2AgBiBr_6$ was calculated to be 167 meV within effective mass theory, which is sufficiently large that stable exciton formation is possible in these systems.

Curiously, the computed absorption spectrum for $Cs_2AgSbBr_6$ shows a distinct absorption peak (Fig. 4f), whereas the measured peak from UV-visible spectrophotometry became less

distinct with increasing Sb content, until there was barely an observable peak for the pure Sb-based compound (Fig. 3a). This may have been due a 'smearing out' of the absorption peak due to structural disorder.[56–58] We calculated the absorption spectra for the pure Sb-based compound convoluted with Gaussian peaks with wider FWHM (0.2 eV, 0.3 eV, 0.4 eV; Fig. S16, ESI‡). These show that the peak becomes indistinguishable when broadening is large, as witnessed experimentally and consistent with the PDS measurements. Thus, peak broadening as a result of disorder leads to the observed 'smeared-out' absorption spectrum in Fig. 3a.

Conclusions

In conclusion, we successfully synthesized phase-pure $Cs_2AgSbBr_6$ thin films, as well as $Cs_2Ag(Sb_xBi_{1-x})Br_6$ with x varying over the full composition range. In doing so, we found that the mixed double perovskites with x between 0.5 and 0.9 to have the smallest bandgaps, lower than those of the pure compounds. From the electronic band alignment, we found that the origin of bandgap bowing in this double perovskite alloy is due to chemical rather than structural effects. The type II band alignment between $Cs_2AgBiBr_6$ and $Cs_2AgSbBr_6$, in combination with non-linear mixing of the electronic states, results in the alloy having smaller bandgaps than either pure material. Our work demonstrates a novel route to reduce the bandgap of $Cs_2AgBiBr_6$ and $Cs_2AgSbBr_6$, which could be generalized to other halide double perovskites. That is, we propose that alloys formed from compounds with a type II band alignment could exhibit similar bandgap lowering. This may prove crucial for improving the suitability of double perovskites for photovoltaic and photocatalytic applications.

Author contributions

Z. L. synthesized the Sb–Bi double perovskite thin films, took photographs, and performed 1D XRD, SEM and UV-visible spectrophotometry measurements. S. R. K. performed the theoretical calculations and analyzed the results, along with D. W. D., D. O. S. and A. W. M. N. analyzed the RBS results, which were collected by M. L. and J. J. R. G. P. measured the 2D XRD data. M. A.-J. and Z. A.-G. measured and analyzed the PDS data. M. I. performed the PES measurements. R. H. F. supervised Z. L. and contributed to the discussion. R. L. Z. H. conceived of the project and supervised the work. All authors discussed the results and contributed to writing the paper.

Conflicts of interest

There are no conflicts of interest to declare.

Acknowledgements

21786 | *J. Mater. Chem. A*, 2020, **8**, 21780–21788

This journal is © The Royal Society of Chemistry 2020

References

1 L. Yang, A. T. Barrows, D. G. Lidzey and T. Wang, *Rep. Prog. Phys.*, 2016, **79**, 026501.

2 H. S. Jung and N. G. Park, *Small*, 2015, **11**, 10–25.

3 A. Babayigit, A. Ethirajan, M. Muller and B. Conings, *Nat. Mater.*, 2016, **15**, 247–251.

4 S. Nagane, D. Ghosh, R. L. Z. Hoye, B. Zhao, S. Ahmad, A. B. Walker, M. Saiful Islam, S. Ogale and A. Sadhanala, *J. Phys. Chem. C*, 2018, **122**, 5940–5947.

5 R. E. Brandt, J. R. Poindexter, P. Gorai, R. C. Kurchin, R. L. Z. Hoye, L. Nienhaus, M. W. B. Wilson, J. A. Polizzotti, R. Sereika, R. Žaltauskas, L. C. Lee, J. L. Macmanus-Driscoll, M. Bawendi, V. Stevanović and T. Buonassisi, *Chem. Mater.*, 2017, **29**, 4667–4674.

6 A. Walsh, D. O. Scanlon, S. Chen, X. G. Gong and S. H. Wei, *Angew. Chem. Int. Ed.*, 2015, **54**, 1791–1794; *Angew. Chem.*, 2015, **127**, 1811–1814.

7 F. Wei, Z. Deng, S. Sun, F. Zhang, D. M. Evans, G. Kieslich, S. Tominaka, M. A. Carpenter, J. Zhang, P. D. Bristowe and A. K. Cheetham, *Chem. Mater.*, 2017, **29**, 1089–1094.

8 C. N. Savory, A. Walsh and D. O. Scanlon, *ACS Energy Lett.*, 2016, **1**, 949–955.

9 F. Wei, Z. Deng, S. Sun, F. Xie, G. Kieslich, D. M. Evans, M. A. Carpenter, P. Bristowe and T. Cheetham, *Mater. Horiz.*, 2016, **3**, 328–332.

10 Z. Xiao, W. Meng, J. Wang and Y. Yan, *ChemSusChem*, 2016, **9**, 2628–2633.

11 G. Volonakis, M. R. Filip, A. A. Haghighirad, N. Sakai, B. Wenger, H. J. Snaith and F. Giustino, *J. Phys. Chem. Lett.*, 2016, **7**, 1254–1259.

12 E. T. McClure, M. R. Ball, W. Windl and P. M. Woodward, *Chem. Mater.*, 2016, **28**, 1348–1354.

13 A. H. Slavney, T. Hu, A. M. Lindenberg and H. I. Karunadasa, *J. Am. Chem. Soc.*, 2016, **138**, 2138–2141.

14 J. Luo, X. Wang, S. Li, J. Liu, Y. Guo, G. Niu, L. Yao, Y. Fu, L. Gao, Q. Dong, C. Zhao, M. Leng, F. Ma, W. Liang, L. Wang, S. Jin, J. Han, L. Zhang, J. Etheridge, J. Wang, Y. Yan, E. H. Sargent and J. Tang, *Nature*, 2018, **563**, 541–545.

15 F. Wei, Z. Deng, S. Sun, N. T. P. Hartono, H. L. Seng, T. Buonassisi, P. D. Bristowe and A. K. Cheetham, *Chem. Commun.*, 2019, **55**, 3721–3724.

16 R. L. Z. Hoye, L. Eyre, F. Wei, F. Brivio, A. Sadhanala, S. Sun, W. Li, K. H. L. Zhang, J. L. MacManus-Driscoll, P. D. Bristowe, R. H. Friend, A. K. Cheetham and F. Deschler, *Adv. Mater. Interfaces*, 2018, **5**, 1800464.

17 D. Bartesaghi, A. H. Slavney, M. C. Gélvez-Rueda, B. A. Connor, F. C. Grozema, H. I. Karunadasa and T. J. Savenije, *J. Phys. Chem. C*, 2018, **122**, 4809–4816.

18 E. Greul, M. L. Petrus, A. Binek, P. Docampo and T. Bein, *J. Mater. Chem. A*, 2017, **5**, 19972–19981.

19 F. Igbari, R. Wang, Z. K. Wang, X. J. Ma, Q. Wang, K. L. Wang, Y. Zhang, L. S. Liao and Y. Yang, *Nano Lett.*, 2019, **19**, 2066–2073.

20 L. Zhou, Y. F. Xu, B. X. Chen, D. Bin Kuang and C. Y. Su, *Small*, 2018, **14**, 1703762.

21 Z. Zhang, Y. Liang, H. Huang, X. Liu, Q. Li, L. Chen and D. Xu, *Angew. Chem. Int. Ed.*, 2019, **58**, 7263–7267; *Angew. Chem.*, 2019, **131**, 7341–7345.

22 M. R. Filip, S. Hillman, A. A. Haghighirad, H. J. Snaith and F. Giustino, *J. Phys. Chem. Lett.*, 2016, **7**, 2579–2585.

23 H. Huang, B. Pradhan, J. Hofkens, M. B. J. Roeffaers and J. A. Steele, *ACS Energy Lett.*, 2020, **5**, 1107–1123.

24 A. H. Slavney, L. Leppert, D. Bartesaghi, A. Gold-Parker, M. F. Toney, T. J. Savenije, J. B. Neaton and H. I. Karunadasa, *J. Am. Chem. Soc.*, 2017, **139**, 5015–5018.

25 K. Z. Du, W. Meng, X. Wang, Y. Yan and D. B. Mitzi, *Angew. Chem. Int. Ed.*, 2017, **56**, 8158–8162; *Angew. Chem.*, 2017, **129**, 8270–8274.

26 E. M. Hutter, M. C. Gélvez-Rueda, D. Bartesaghi, F. C. Grozema and T. J. Savenije, *ACS Omega*, 2018, **3**, 11655–11662.

27 Y. Liu, L. Zhang, M. Wang, Y. Zhong, M. Huang, Y. Long and H. Zhu, *Mater. Today*, 2019, **28**, 25–30.

28 A. Goyal, S. McKechnie, D. Pashov, W. Tumas, M. Van Schilfgaarde and V. Stevanović, *Chem. Mater.*, 2018, **30**, 3920–3928.

29 G. E. Eperon, T. Leijtens, K. A. Bush, R. Prasanna, T. Green, J. T. W. Wang, D. P. McMeekin, G. Volonakis, R. L. Milot, R. May, A. Palmstrom, D. J. Slotcavage, R. A. Belisle, J. B. Patel, E. S. Parrott, R. J. Sutton, W. Ma, F. Moghadam, B. Conings, A. Babayigit, H. G. Boyen, S. Bent, F. Giustino, L. M. Herz, M. B. Johnston, M. D. McGehee and H. J. Snaith, *Science*, 2016, **354**, 861–865.

30 J. Im, C. C. Stoumpos, H. Jin, A. J. Freeman and M. G. Kanatzidis, *J. Phys. Chem. Lett.*, 2015, **6**, 3503–3509.

31 B. Yang, F. Hong, J. Chen, Y. Tang, L. Yang, Y. Sang, X. Xia, J. Guo, H. He, S. Yang, W. Deng and K. Han, *Angew. Chem. Int. Ed.*, 2019, **58**, 2278–2283; *Angew. Chem.*, 2019, **131**, 2300–2305.

This journal is © The Royal Society of Chemistry 2020

J. Mater. Chem. A, 2020, **8**, 21780–21788 | **21787**

32 M. Gao, C. Zhang, L. Lian, J. Guo, Y. Xia, F. Pan, X. Su, J. Zhang, H. Li and D. Zhang, *J. Mater. Chem. C*, 2019, **7**, 3688–3695.

33 R. L. Z. Hoye, R. E. Brandt, A. Osherov, V. Stevanovic, S. D. Stranks, M. W. B. Wilson, H. Kim, A. J. Akey, J. D. Perkins, R. C. Kurchin, J. R. Poindexter, E. N. Wang, M. G. Bawendi, V. Bulovic and T. Buonassisi, *Chem.–Eur. J.*, 2016, **22**, 2605–2610.

34 R. D. Raninga, R. A. Jagt, S. Béchu, T. N. Huq, W. Li, M. Nikolka, Y. H. Lin, M. Sun, Z. Li, W. Li, M. Bouttemy, M. Frégnaux, H. J. Snaith, P. Schulz, J. L. MacManus-Driscoll and R. L. Z. Hoye, *Nano Energy*, 2020, **75**, 104946.

35 D. E. Sweenor, S. K. O'Leary and B. E. Foutz, *Solid State Commun.*, 1999, **110**, 281–286.

36 T. M. Mok and S. K. O'Leary, *J. Appl. Phys.*, 2007, **102**, 113525.

37 S. S. Shin, S. J. Lee and S. Il Seok, *Adv. Funct. Mater.*, 2019, **29**, 1–30.

38 L. C. Lee, T. N. Huq, J. L. Macmanus-Driscoll and R. L. Z. Hoye, *APL Mater.*, 2018, **6**, 084502.

39 K. G. Stamplecoskie, J. S. Manser and P. V. Kamat, *Energy Environ. Sci.*, 2015, **8**, 208–215.

40 F. Hao, C. C. Stoumpos, D. H. Cao, R. P. H. Chang and M. G. Kanatzidis, *Nat. Photonics*, 2014, **8**, 489–494.

41 L. C. Tang, C. S. Chang and J. Y. Huang, *J. Phys.: Condens. Matter*, 2000, **12**, 9129–9143.

42 K. T. Butler, C. H. Hendon and A. Walsh, *J. Am. Chem. Soc.*, 2014, **136**, 2703–2706.

43 D. R. Lide, *CRC Handbook of Chemistry and Physics*, CRC Press, Florida, 84th edn, 2003, ch. 10.

44 P. Pyykkö, *Chem. Rev.*, 1988, **88**, 563–594.

45 S. H. Wei and A. Zunger, *Phys. Rev. B: Condens. Matter Mater. Phys.*, 1989, **39**, 3279–3304.

46 C. Y. Moon, S. H. Wei, Y. Z. Zhu and G. D. Chen, *Phys. Rev. B: Condens. Matter Mater. Phys.*, 2006, **74**, 233202.

47 T. Mattila, S. H. Wei and A. Zunger, *Phys. Rev. B: Condens. Matter Mater. Phys.*, 1999, **60**, R11245–R11248.

48 A. Goyal, P. Gorai, S. Anand, E. S. Toberer, G. J. Snyder and V. Stevanović, *Chem. Mater.*, 2020, **32**, 4467–4480.

49 A. Schleife, F. Fuchs, C. Rödl, J. Furthmüller and F. Bechstedt, *Appl. Phys. Lett.*, 2009, **94**, 012104.

50 A. Zunger, *Appl. Phys. Lett.*, 2003, **83**, 57–59.

51 Z. Zhang, G. Yang, C. Zhou, C. C. Chung and I. Hany, *RSC Adv.*, 2019, **9**, 23459–23464.

52 W. Gao, C. Ran, J. Xi, B. Jiao, W. Zhang, M. Wu, X. Hou and Z. Wu, *ChemPhysChem*, 2018, **19**, 1696–1700.

53 R. Kentsch, M. Scholz, J. Horn, D. Schlettwein, K. Oum and T. Lenzer, *J. Phys. Chem. C*, 2018, **122**, 25940–25947.

54 S. J. Zelewski, J. M. Urban, A. Surrente, D. K. Maude, A. Kuc, L. Schade, R. D. Johnson, M. Dollmann, P. K. Nayak, H. J. Snaith, P. Radaelli, R. Kudrawiec, R. J. Nicholas, P. Plochocka and M. Baranowski, *J. Mater. Chem. C*, 2019, **7**, 8350–8356.

55 L. Schade, A. D. Wright, R. D. Johnson, M. Dollmann, B. Wenger, P. K. Nayak, D. Prabhakaran, L. M. Herz, R. Nicholas, H. J. Snaith and P. G. Radaelli, *ACS Energy Lett.*, 2019, **4**, 299–305.

56 S. S. Savchenko and I. A. Weinstein, *Nanomaterials*, 2019, **9**, 716.

57 I. A. Weinstein, A. F. Zatsepin and V. S. Kortov, *J. Non-Cryst. Solids*, 2001, **279**, 77–87.

58 R. Butté, L. Lahourcade, T. K. Uzdavinys, G. Callsen, M. Mensi, M. Glauser, G. Rossbach, D. Martin, J. F. Carlin, S. Marcinkevičius and N. Grandjean, *Appl. Phys. Lett.*, 2018, **112**, 032106.

21788 | *J. Mater. Chem. A*, 2020, **8**, 21780–21788

This journal is © The Royal Society of Chemistry 2020